Applied Physics A (2023) 129:95
https://doi.org/10.1007/s00339-022-06304-3

Applied Physics A
Materials Science & Processing

S.I. : 50TH ANNIVERSARY OF APPLIED PHYSICS

Electromechanical and electrochemical properties of highly filled Titanium composites for PEM bipolar plates

Maria Gaudig[1] · Wolfram Münchgesang[2] · Juliana Martins de Souza e Silva[1,3] · Fabian Pascher[2] · Thorsten Hickmann[4] · Ralf B. Wehrspohn[1]

Received: 18 October 2022 / Accepted: 28 November 2022 / Published online: 10 January 2023

Abstract
Titanium polymer composites are evaluated concerning their suitability as bipolar plates in acid water electrolysis as a replacement of milled Titanium bipolar plates. It turns out that our highly filled polymer composites with 80 wt.-% Titanium powder meet all criteria given by US Department of Energy concerning electric conductivity and mechanical stability. Concerning the electrochemical corrosion test, an improved behavior is obtained by coating the composites by a 0.5 μm thin Titanium layer. The coated Titanium composite bipolar plate has been successfully integrated in a PEM fuel cell. The polarization curves show good electrolysis performances for short time, but further improvements on the coating and the surface roughness need to be made for long-time stability.

Keywords Bipolar plates · Electrolysis · Composite · Elctrochemical · Mechanical · Hydrogen production

1 Introduction

The worldwide hydrogen consumption has increased continuously in the last few decades from around 18 Mt in 1975 to around 90 Mt in 2020. The demand will very likely continue to rise, even more strongly, because hydrogen is becoming more and more attractive as a sustainable energy carrier [1–3]. In terms of generation, about 96% of the global amount of hydrogen is currently obtained from fossil raw materials, e.g., through natural gas steam reforming, which in 2018 caused about 830 Mt of carbon dioxide emission as a by-product during the generation process and through coal and natural gas extraction and transport. This amount is roughly equivalent to the CO_2 emissions of an industrial nation like Germany [4–6]. For a sustainable "green" hydrogen production, water splitting by electrolysis technologies is more and more sought after. In particular, the Proton Exchange Membrane (PEM) electrolysis is interesting for coupling with intermittent renewable energy sources, as it offers fast ramp-up times and works in a wide partial load range. Further advantages are the compact design, a higher power density and gas purity compared to alkaline electrolysis. However, the main obstacles to the establishment of PEM electrolysis are the high costs and low durability [7]. One component in the PEM electrolyzer is particularly expansive and accounts for around 50% of the stack costs and around 25% of the total system costs: the bipolar plates (BPPs) that separate the individual electrochemical cells and function as current and heat conductors [8–10]. To withstand the extreme electrochemical loads of a low pH value of around 2 and a high voltage of up to 2 V during electrolysis, titanium or stainless steel is used as material for the plates, which are expensive to purchase, manufacture and process (e.g., by milling) [11]. In the case of stainless steels, the necessary surface refinement to improve the chemical stability causes additional costs. To significantly increase the economic efficiency of PEM electrolyzers, it is, therefore, urgently necessary to develop more cost-effective materials as well as manufacturing processes for BPPs. For this

✉ Ralf B. Wehrspohn
ralf.wehrspohn@physik.uni-halle.de

1 Group µMD, Institute of Physics, Martin Luther University Halle-Wittenberg, Heinrich-Damerow-Str. 4, 06120 Halle (Saale), Germany

2 Fraunhofer Institute for Wind Energy Systems IWES, Am Haupttor 4310, 06237 Leuna, Germany

3 Fraunhofer Institute for Microstructure of Materials and Systems IMWS, Walter-Hülse-Straße 1, 06120 Halle (Saale), Germany

4 Eisenhuth GmbH, Friedrich-Ebert-Straße 203, 37520 Osterode Am Harz, Germany

Table 1 Composition of prepared and characterized plates

Ti powder content in wt.-%	PVDF 705	PVDF 720
70	Ti70-P705	
80	Ti80-P705	Ti80-P720
90	Ti90-P705	Ti90-P720

purpose, various approaches are being investigated. Inexpensive coatings and deposition technologies are being studied intensively to protect plates, especially made of stainless steel, which are easier to deform compared to titanium plates [8, 12–14]. In addition, new BPP concepts are proposed, with additive manufacturing and 3D printing [15–17].

Recently, a titanium-coated molded graphite conductive plastic BP for use in PEM electrolysis cells was presented [18]. Composite BPPs have already been evaluated as cost effective for PEM fuel cells; their fillers consist of graphite or carbon [19–21], which cannot be used (uncoated) as anode in PEM electrolysis cells due to the material degradation at the higher voltage during water splitting. The use of composite materials as BPP material instead of full metal BPP is advantageous because, in addition to the material cost savings through the partial use of a cheap polymer, processing and end plate molding can be achieved by hot pressing or injection molding, which enables further savings in production costs [22]. In this context, this work presents a new type of Ti composite as an alternative material to conventional metal BPPs for PEM electrolyzers. Here, we present and discuss the three-dimensional (3D) microstructural, electrical, mechanical and electrochemical properties of this highly filled and astonishingly conductive composite with different metal–polymer compositions. We furthermore discuss how microstructures and morphology might correlate with the macroscopic properties of the composite. As result of the experiments, we found that the composite composition with 80 wt.-% Ti meets all requirements as a PEM electrolysis BPP. Thus, we manufactured composite BPPs with this composition, integrated it into a standard electrolysis cell and tested in an electrolyzer test stand with a protective titanium coating. Our results were compared with identical measurements from an electrolysis cell with standard Ti BPPs and we found that the composite BPP cell achieve promising initial performance but still have further potential for optimization.

2 Experimental

Material and BPPs preparation The manufacturing process of the composites was developed and carried out by Eisenhuth GmbH. A polymer powder as well as a Ti powder are mixed and compounded. Hot compression is carried out to fabricate the final form. Two commercially available thermoplastic fluoropolymers, polyvinylidene fluoride (PVDF) powders Kynar 705® and Kynar 720®, were used to prepare five plates with the composition as listed in Table 1. The diameter of the plates is approximately 19 cm and the thicknesses are about 5 mm. In addition, BPPs were prepared for the PEM electrolyzer test station. The final forms and the flow fields are realized by a milling process.

Protective coating The sample coating with titanium was carried out using two different sputtering tools. A PECS ™ (Precision ion polishing system) tool from Gatan was used to coat small samples for electrochemical analyzes (size: approx. 2 * 1.5 cm^2). The layer growth is about 0.14 nm/s at the set energy of the argon ions of about 10 keV. In order not to overheat the target, the deposition process is interrupted after each 50 nm and restarted after a short pause to cool down.

A magnetron sputterer with a 4-inch chamber was used to coat the large BPPs. The deposition rate here is about (0.3–0.5) nm/s. With this device, too, the coating was interrupted after a few minutes in order not to overheat the samples in the chamber. SEM images of the homogeneously coated surface are shown in Fig. 1d) and 1e).

Surface analysis The microstructure of the surfaces was examined with scanning electron microscopy (SEM). The ESEM™ mode of a Philips XL30 ESEM FEG microscope and the low voltage range of a FEI Versa 3D DualBeam™ microscope were used to avoid charging effects of the polymer.

To characterize the surface roughness, line scans with a length of 5 mm were carried out with an Ambios XP-2 ™ Profiler. The arithmetical mean deviations ($Ra = \frac{1}{L}\int_0^L |z(x)|dx$ with the length L and the height profile $z(x)$) and the highest peak-valley distances (Rt) are calculated from these profiles. At least six different spots on the plates were investigated.

3D microstructure analysis The samples, cut as 5 * 5 * 5 mm^3, were imaged using absorption contrast X-ray micro-computed tomography (micro-CT) in a GE phoenix nanome|x (Tungsten source, 120 kV and 35 mA) with variable source-sample and sample-detector distances that resulted in pixel sizes that slightly varied among samples. For each sample, a total of 1001 projection images with an exposure time of 800 ms each was acquired by rotation over 360°. Image reconstruction was performed by filtered back-projection algorithm using the GE phoenix datos|x software integrated into the device. The tomograms obtained were exported as a stack of 16-bit TIFF images of 1000 * 1000 pixels for further processing.

Electrical characterization The electrical conductivity was measured using a 4-point-probe at various spots (at least five different) on the plate surfaces. The needle distance is 5 mm.

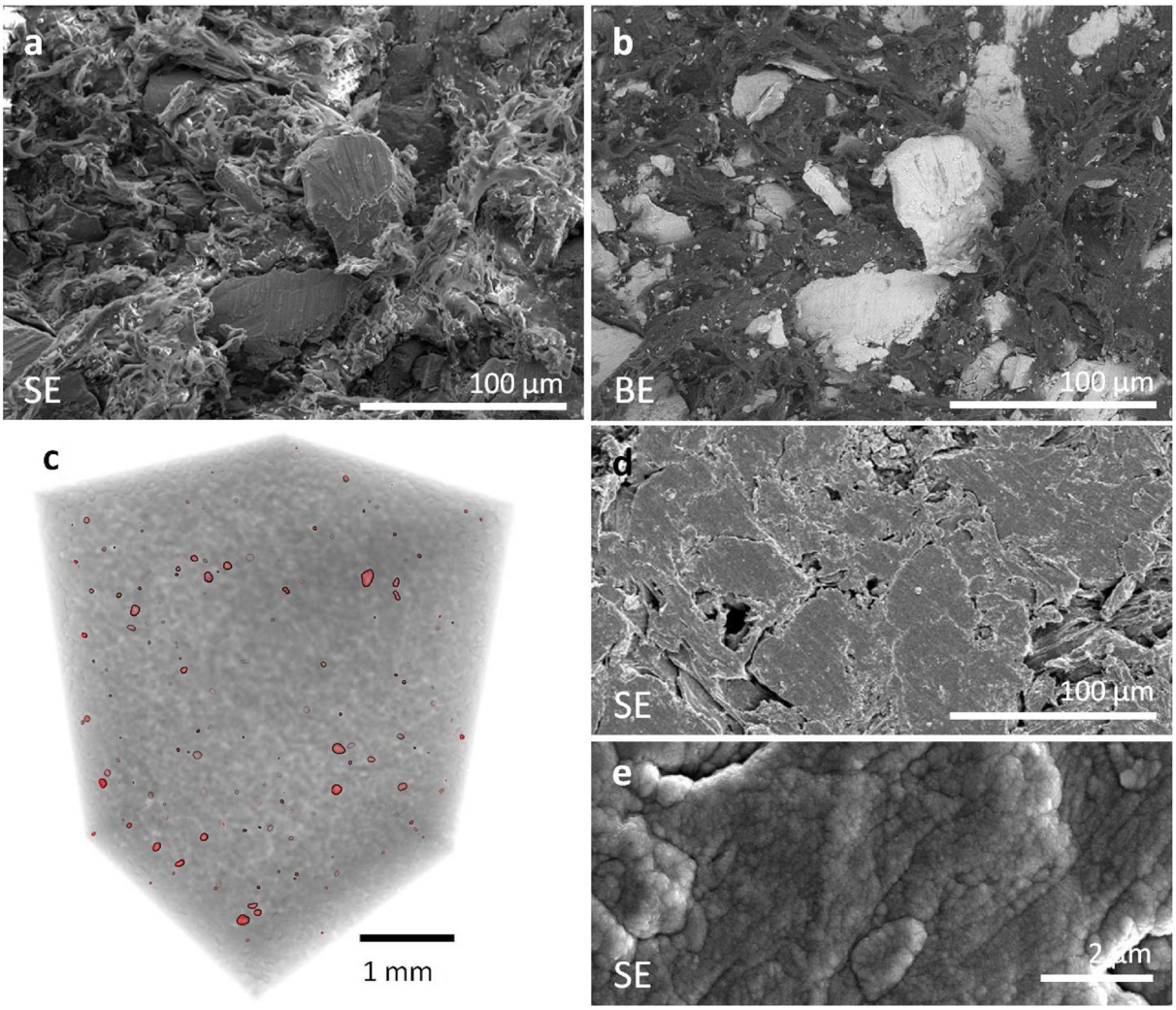

Fig. 1 Microstructure characterization. SEM images of the Ti80-P705 composite, recorded simultaneously with **a** a secondary electron detector (SE) for the topology contrast and **b** with a back-scattered electron detector (BE) for the material contrast. **c** Micro-CT volumetric reconstruction of sample Ti90-P705, with Ti particles marked in red within a gray pseudo-transparent cube of polymer. **d**, **e** SEM image of a Ti80-P705 composite BPP after deposition of 700 nm titanium

Mechanical tests For the compressive load tests with a Zwick Z050 tool and a load cell with 50 kN, the stress–strain curves were measured of five samples with an area of 10 * 4 mm^2 for each plate. The Young's modulus and the compressive strength are calculated according to the DIN EN ISO 604 standard from these curves. Furthermore, three-point bending tests according to the DIN ISO 527 standard were performed to calculate the flexural strength with a tool from Hegewald & Peschke and a load cell with 10 kN. At least five samples of each composition with a length of 120 mm were examined.

Electrochemical corrosion test The corrosion resistance of the composite material compared to pure Ti (grade 2) was evaluated by determining the corrosion potential E_{corr}, the corrosion current density j_{corr} before and after an electrochemical corrosion stress test under PEM environmental conditions. For this purpose, the potentiodynamic polarization curve were measured by linear voltammetry scan performed at 1 mV/s and analyze by the Tafel method using the Gamry Echem Analyst software to determine the evaluation parameters. The corrosion test was performed potentiostatically at a voltage of 2 V for 3 h. The measurements were carried out with a Gamry 600 potentiostat in a corrosion cell at 60 °C, in an oxygen saturated 0.5 mol H_2SO_4 solution with the sample as working electrode (sample area 5 * 10 mm^2), a platinum counter electrode and a reversible hydrogen electrode as reference. Before the test, all samples were cleaned in a ultrasonic bath with water and isopropyl alcohol.

PEM electrolyzer test The electrolysis tests were carried out in a Greenlight Innovation test stand Series E in combination with a 50 cm^2 large baticfuelcells quick connect electrolysis cell. Ti BPP (grade 2) with a parallel flow field

were used for the measurement as well as for each test new porous transport layers of carbon paper on the cathode side and a titanium fleece on the anode side, a catalyst coated membrane of Nafion 115 with a loading of 1 mg/cm^2 Pt/C on the cathode and 2 mg/cm^2 Iridium black on the anode. For the performance comparison, the anode BPP was replaced by a geometrically identical Ti-coated composite BPP.

The following test protocol was carried out for the comparison measurements: 1) break-in phase: the cell was potentiostatically conditioned at two voltages, 1.8 V and 2 V, for 30 min each; 2) performance evaluation at the beginning of the test (BoT): galvanostatic polarization curves (PC) in steps of 120 s at 80, 60 and 40 °C up to the termination voltage of 2.2 V; 3) galvanostatic stress test at 1 A/cm^2 for 24 h or up to 2.1 V; 4) performance evaluation at the end of the test (EoT), like BoT. After measurement, the PCs were analyzed with a regression model according Santarelli et al. [23] (without mass transport) using the Levenberg–Marquardt algorithm implemented in the LMFIT python library [24] to extract the ohmic cell resistance.

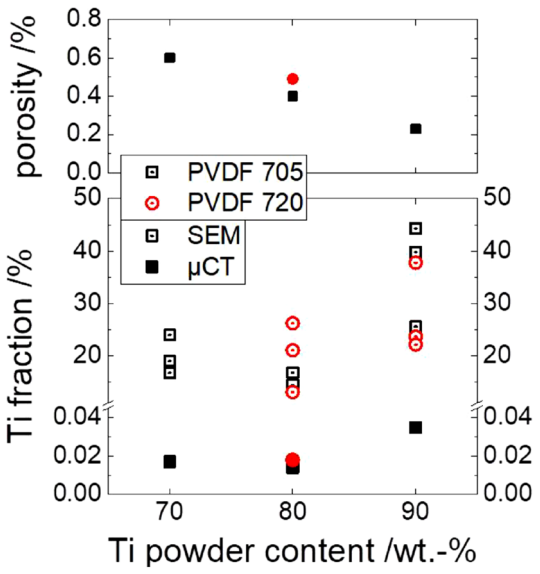

Fig. 2 Composition. Porosity and Ti fraction of the volume (filled symbols indicate data calculated from micro-CT volumetric images) and of the surface (open symbols indicate data calculated from SEM images) depending on the Ti powder content during manufacturing

3 Results and discussion

3.1 Microstructure, composition and roughness

Examplary SEM images of the composites surface are shown for the Ti80-P705 plate (Fig. 1). On Fig. 1b), the image contrast clearly highlights the metal particles (brighter areas) of different sizes ranging from 1 to 100 μm, which are embedded in the polymer matrix. The topology of the rough surface appears in Fig. 1a), with smooth Ti particles and fibrous polymer chains. A characteristic volumetric image by X-ray micro-CT imaging is shown in Fig. 1c) and a movie going through tomographic slices of a composite can be found in the supplementary files. The 3D scans show that the particles are homogeneously distributed throughout the volume of analysis.

We used the 3D micro-CT images to calculate the porosity and volumetric composition of the samples. In addition, we calculated the Ti surface fraction from the SEM images at three different spots on each sample (image size: $\approx$ 2100 * 1400 μm^2), which are plotted in Fig. 2. With regard to the porosity determined from micro-CT analyzes, the samples are relatively non-porous with values below 1% and, in addition, the porosity decreases with a higher Ti powder content to about 0.2% for 90 wt.-%. Thus, a high Ti content is preferred for a low porosity in order to meet the dense material requirements for BPPs with low hydrogen diffusion. The calculations of the composition show that the Ti surface fraction is highest in the samples with a 90 wt.-% Ti content, as expected. However, the proportion for the concentrations 70 wt.-% and 80 wt.-% remains the same. In addition, the volume fraction data at least confirm the Ti fraction trend just explained, although the resolution of the micro-CT is limited to some microns and only Ti particles with a size larger than 3 μm could be resolved, as already shown in Fig. 1c).

One surface profile per sample analyzed by a profilometer is shown in Fig. 3, together with the dependence of Ra and Rt on the composition on the right-hand side. It is evident from these diagrams that, if more Ti powder is used as a filler, the surface becomes rougher. While the composite with 90 wt.-% Ti is very rough with a value for Ra of 20 μm and Rt up to 100 μm, the Ti70-P705 sample is much smoother (Ra value $\approx$ 4 μm) with smaller peak-valley distances up to 40 μm. For comparison, the Ra and Rt values for a similarly manufactured Ti plate are illustrated as well; these values are comparable to the composition with 70 wt.-%.

The investigation of the surface roughness of BPPs is important, as this property has a decisive influence on the water management and the conductivity of fuel cells [25–27]. A very rough surface can increase the contact resistance and also damage the membrane or other cell components [26, 28, 29]. Regarding Ra and Rt in Fig. 3, the curves depending on the Ti powder concentration are similar to the trend of the Ti fraction in Fig. 2, even the high inhomogeneity for the 90 wt.-% samples is consistent. This correlation between filler concentration and roughness was also shown, for example, by Upadhyay et al. [30]. Thus, to meet smooth surfaces as requirement for BPPs, a lower Ti

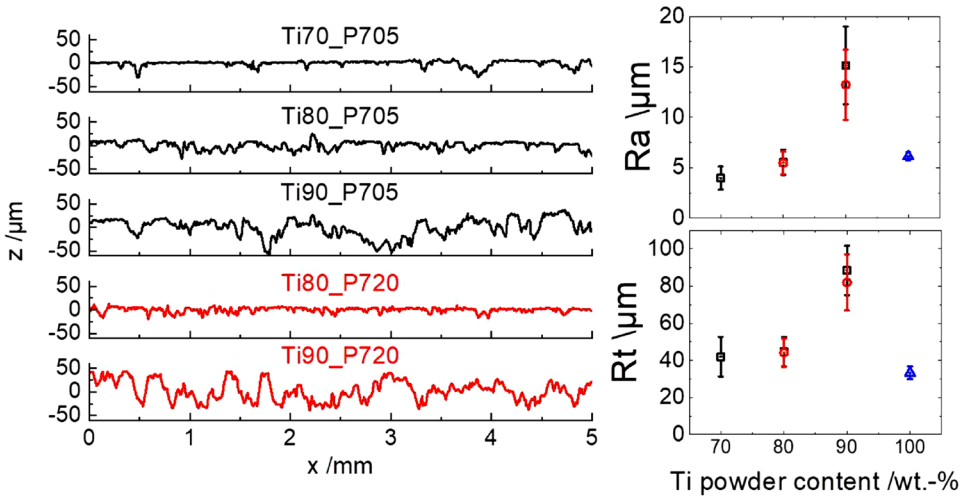

Fig. 3 Surface roughness. Left: Profile curves of the composite surfaces measured by a profilometer. Right: Calculated values of Ra and Rt are plotted (mean and standard deviation)

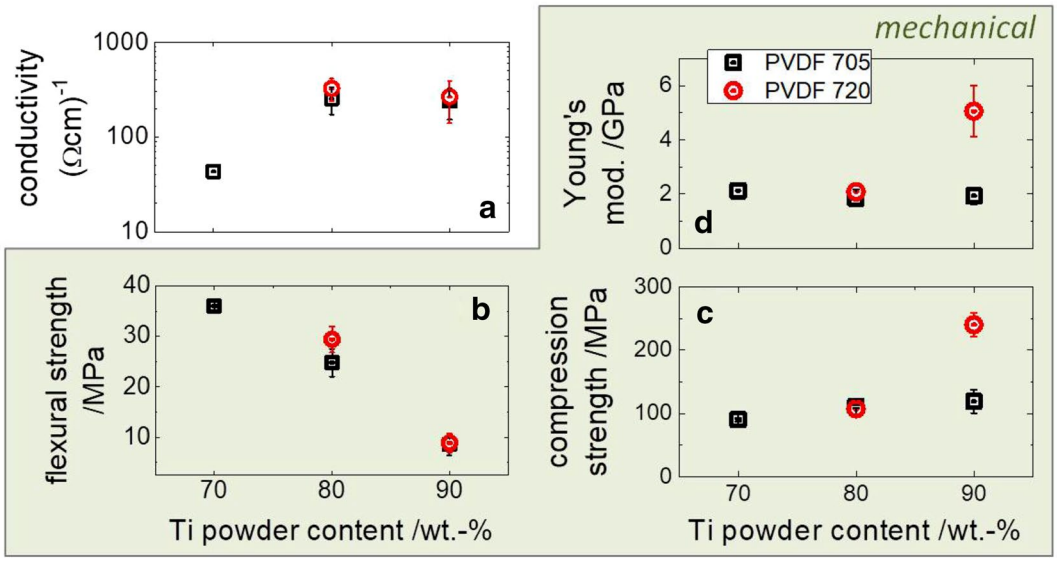

Fig. 4 Electromechanical properties. a The electrical conductivity, **b** the flexural strength, **c** the compressive strength and **d** the Young's modulus for the different composite plates

powder concentration is obviously preferable to reduce the roughness and inhomogeneity for this composite material.

According to the study by San et al. the optimal value range of the roughness is between 0.44 μm and 2.08 μm depending on the other cell components [26]. This range is consistent with other research results [25, 27, 31]. For our samples with a minimum Ra value of about 4 μm, a final surface polishing for smoother samples could be useful as a future task in order to improve the electrolysis performance.

3.2 Electrical conductivity

The results of the electrical conductivity measurements are plotted in Fig. 4a). To use the Ti composite as BPP, the US Department of Energy recommends a conductivity above 100 $(\Omega cm)^{-1}$, which is met for Ti-Powder contents equal to or higher than 80 wt.-% [32]. The material reaches relatively high values between 240 $(\Omega cm)^{-1}$ and 330 $(\Omega cm)^{-1}$ compared to other investigated metal or carbon-based composites [33, 34]. The conductive network is apparently optimally connected for a Ti powder content of about 80 wt.- %, since the conductivity does not increase with more Ti. With a Ti content of 70 wt.-%, an enormous drop in conductivity occurs, which suggests a severely weakened electrically conductive network [35]. This decrease cannot be explained by a reduced metal concentration, which would certainly be the most intuitive explanation, since the Ti fraction of these two samples is similar (Fig. 2).

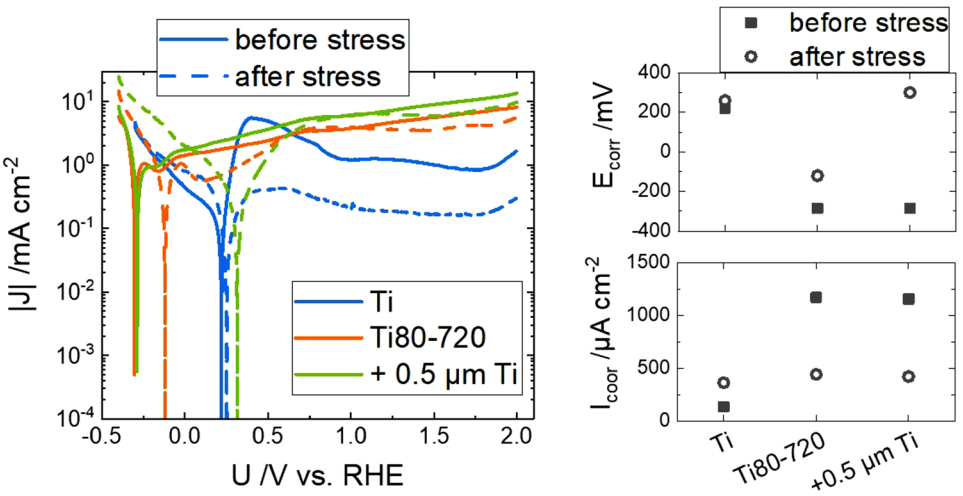

Fig. 5 Electrochemical corrosion properties. Left: Polarization curves of a Ti sample (blue) and two Ti80-720 composites, without (orange) and with a 500 nm thin Ti layer (green) before (solid line) and after (dashed line) the corrosion stress test. Right: The respective values for the corrosion potential and corrosion current density before and after the stress test

However, other characteristic parameters also influence the electrical conductivity of composite materials, which have been extensively investigated for example by Radzuan et al. [36]. Based on this study, it is assumed here that the reason for the reduced conductivity is the increased porosity and probably a different Ti-PVDF interphase, since the same filler and polymer powder as well as the same manufacturing method were used for all samples.

3.3 Mechanical stability

The BPPs must withstand a certain pressure load up to 80 bar during the electrolysis process. However, they must also be flexible to a certain extent, as pressure gradients occur along the cell surface during water splitting. To investigate whether our composite plates meet both properties, we applied compressive load and bending tests. For the compressive load test, the Young's modulus and the compressive strength are calculated from measured stress–strain curves (Fig, 4c and d). All compositions reach similar values of about 2 GPa for Young's modulus and about (90–120) MPa for the compressive strength, with the exception of those for the Ti90-P720 sample that achieves values about 2.5 times higher. These characteristics are sufficient to withstand the compression forces in the cell.

A three-point bending test was used to evaluate the flexural strength, which are plotted in Fig. 4b) for our samples. The bending parameter decreases with higher Ti content; the material becomes less flexible. According to the US Department of Energy, a sufficient flexural strength over 25 MPa is required so that BPPs can withstand bending moments during electrolysis [32]. This requirement is fulfilled here for Ti concentrations equal to or less than 80 wt.-% (Fig. 4b)). With a higher Ti powder content, a decrease in flexural strength is observed, which has already been determined in other research studies [35, 37, 38]. Kuan et al. explained this correlation of their graphite–resin composites with a weaker adhesion between filler and resin for a higher graphite content and, furthermore, the higher porosity and voids for a lower filler concentration reduce the bending property, which, all in all, agrees very well with our analysis [35].

3.4 Electrochemical corrosion tests

Figure 5 shows the polarization curves, corrosion potential E_{corr} and corrosion current J_{corr} before and after the stress tests of the Ti sample, a Ti-coated and an uncoated Ti80-P720 sample as examples for the composite mixtures.

Regarding first the right diagrams of Fig. 5, the Ti sample shows a significantly better corrosion resistance with E_{corr} of 221 mV and J_{corr} of 132 μA/cm^2 compared to the two composite variants. This corrosion resistance can be explained by the natural titanium oxide layer of the titanium [39]. The corrosion potential of the composites, on the other hand, is in the negative range at - 285 mV and the corrosion current densities are about a factor of 9 greater. After the stress test, the corrosion potential of the Ti-coated composite shifted into the positive range, the E_{corr} value of 300 mV is now in the comparable range of the Ti sample of 260 mV in the final state. The corrosion potential of the uncoated variant, on the other hand, is still in the negative range. The current densities of all samples are indistinguishable after the stress tests. This change of the corrosion potential after the stress tests is the result of the formation of a titanium oxide passivation layer on the Ti surfaces. Thus, after the stress test, the corrosion behavior of the Ti reference and the Ti-coated composite are comparable.

Considering the general trend of the curves in the left diagram of Fig. 5, the passivation region (at values greater than 0.9 V vs. RHE) of the Ti sample shows the typical flat behavior, and its intensity decreases after the stress test as

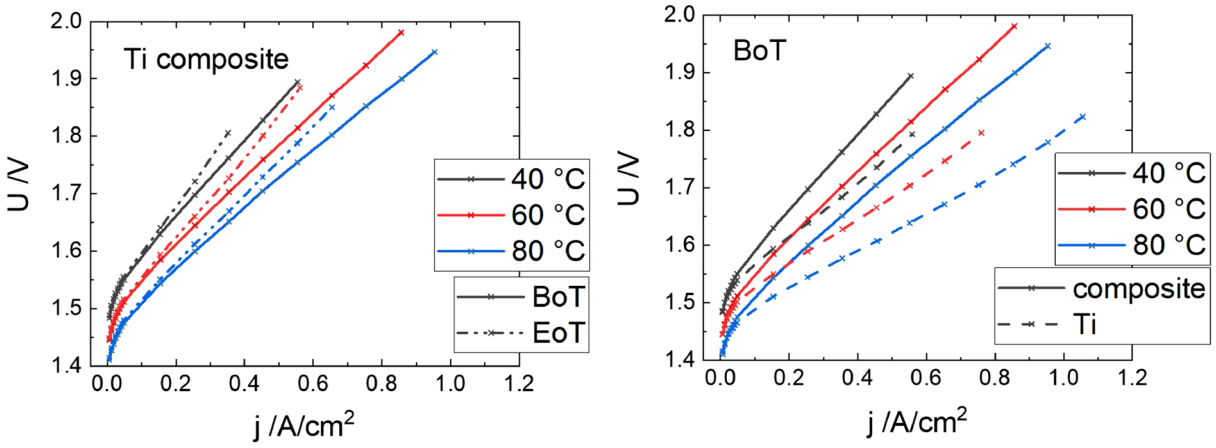

Fig. 6 Temperature-dependent electrolysis performance. Polarization curves at 40 °C (black), 60 °C (red) and 80 °C (blue). Left: Comparison of the cell test set-up with the Ti composite anode at BoT and EoT state. Richt: Comparison of the BoT cell set-up with the Ti anode and the Ti composite anode

expected for a growing passivation layer. In contrast, the passivation regions of the coated and uncoated composite samples are similar showing higher intensities, which do not decrease as much after the stress test as for the Ti sample; moreover, a continuous increase of the current density is observed for the composite samples in this range, which levels off after the stress test. The different trends especially between the Ti sample and the coated composite sample, which should have a comparable passivation behavior at least after the stress test due to the passivating oxide layer and the same corrosion potential, indicate that not only the composition of the surface material influences the passivation range. But, these characteristics are rather attributed to the surface morphology and roughness, which can have a strong influence on the passivation range [18], and in which the composite sample differs from the Ti (see Fig. 3).

After testing, SEM analyses (not shown here) were performed to find out the effects on surface morphology, with the result that no significant changes in surface composition or structure occurred. Further, similar polarization curves and trends are also observed for the other composites, which were tested in the same way. No significant trends or correlation between different Ti powder concentrations and the respective electrochemical properties are observed. However, the samples with an additional titanium coating show a higher corrosion potential (comparable to that of the Ti sample) as the uncoated composite material after the stress test. Thus, to achieve high corrosion resistance, which is required for BPPs, an additional titanium coating should be applied to the composite BBP for protection.

Table 2 Calculated temperature-dependent ohmic resistance of the electrolytic cells with Ti and with Ti composite BPP on the anode in BoT and EoT state and the associated model uncertainty (standard deviation)

T (°C)	Sample state	R_{Ti} (mΩ cm^2)	$R_{composite}$ (mΩ cm^2)	$R_{composite}$ - R_{Ti} (mΩ cm^2)
40	BoT	431 ± 18	594 ± 7	+163
60	BoT	355 ± 12	517 ± 4	+161
80	BoT	306 ± 9	457 ± 2	+151
40	EoT	447 ± 18	723 ± 24	+275
60	EoT	399 ± 21	646 ± 20	+246
80	EoT	342 ± 13	540 ± 9	+197

3.5 PEM electrolysis test

We performed the PEM electrolysis test with a fabricated and Ti coated composite BPP with 80 wt.-% Ti and the polymer PVDF 720, since this composition has the optimal electromechanical properties with similar good conductivities but better flexural strength and a smoother surface compared to the samples with 90 wt.-% Ti.

In Fig. 6 in the left diagram, the temperature-dependent polarization curves are plotted for the BoT and EoT state of the cell set-up with the composite BPP on the anode side. The curves show the typical shape for a PEM water electrolyzer with its three phases: (i) the initial range at low current densities (< 0.15 A/cm^2) which is dominated by the activation losses (Faradaic losses), (ii) the middle, nearly linear current density range (< 1 A/cm^2), which is dominated by the ohmic losses, and (iii) the final range (> 1 A/cm^2), which is influenced by the incipient mass transport losses [40]. Thereby, mass transport losses in region (iii) were neglected, and residual influences in the high-voltage region were deleted manually for the analysis in the illustrated

Table 3 Key data for our Ti and Ti composite material as well as further materials from the literature

Sample composition	Conductivity $(\Omega cm)^{-1}$	Flexural strength (MPa)	Cell performance U at $1A/cm^2$ (V)
Ti80-P720 + 0.5 μm Ti (**this study**)	330 ± 88	30 ± 3	2.0
Titanium (**this study**)	3256 ± 200	–	1.8
Steel SS304[14]	4902	–	–
Steel SS304 + 3.66 μm TiZr [14]	3448	–	–
non-conductive BPP + 50 μm Ti [17]	–	–	2.21 (at 20 °C, 1 atm)
additive manufactured Steel [16]	–	–	1.6 (at 80 °C, 1 atm)
3D printed BPP + coatings [15]	–	–	2.4 (at 80 °C, 7.5Nm)
low-carbon content BPP [34]	420.6	28.4	–
80 wt.-% Ti_3SiC_2-PVDF BPP [37]	29	25	–
Platinum-deposited Ti BPP [43]	105	–	about 1.6

data. Furthermore, the curve shift with changing electrolyte temperatures shows the expected temperature-dependent behavior. The ohmic overvoltage decreases with increasing temperature due to the increase in ionic conductivity of the membrane. The change in 125 $m\Omega\ cm^2$ at a temperature difference of 40 K is within the usual range for a Nafion membrane [41, 42].

The right diagram in Fig. 6 shows the comparison of the electrolysis performance of the cell set-up with the BPP composite anode and that with the BPP titanium anode at the BoT state. The data show no significant deviation of the PC in the first sections. In contrast, significantly higher ohmic resistances occur for the composite BPP set-up in the second section. This difference is independent of the temperatures within the model uncertainty and averages 158 $m\Omega cm^2$, as shown in Table 2.

The following stress test of the cell, which was supposed to run for 24 h, had to be stopped prematurely with the composite BPPs after about 5 h when the break criterion of 2 V was reached, regardless of the temperature. In contrast, the cell with the Ti BPP did not reach the break criterion within the 24 h stress test.

After the stress test, the total ohmic cell resistance increases for both set-ups (see Table 2), although the increase for the Ti BPP set-up is within the model uncertainty. In contrast, the ohmic resistance of the composite BPP set-up increases significantly compared to the BoT condition. Since all components—except for the BPP—are assumed identical, this implies a significant electron transport inhibition over the components' interfaces when using composite BPP. Moreover, the resistance difference decreases with higher temperature. This behavior can be understood as an inhibition of mass transport, indicating a degradation not only of electron-conducting interfaces. Therefore, it follows that the corrosion protection that should be achieved by the Ti surface coating is not successful in the long term. Although this was successful for the smaller samples for corrosion resistance. Thus, incomplete surface coating due to the complex geometry of the BPP is likely responsible for the degradation and a adjusted Ti coating is recommended.

3.6 State-of-the-art evaluation

For comparison with standard metal and new BPP materials, Table 3 shows the key data for the 80 wt.-% Ti composite BPP, the Ti BPP, as well as for other exemplary BPP materials from the literature. Regarding the electrical conductivity and flexural strength, our composite reaches values that lie in the upper or middle value range compared with other composite materials, respectively[1]. Compared to metals, the conductivity of the composite is naturally smaller.

The cell voltage of the Ti BPP cell at 1 A/cm^2 is slightly lower than that of the cell from Jung et al. who used platinum coated Ti BPP, a highly corrosion resistant coating for titanium that is often used as a reference material [43]. The cell voltage of the composite cell is in the middle range in comparison with other new bipolar plate materials from the literature, whose values, however, scatter relatively broadly between 1.6 V and 2.4 V. However, the performance values are difficult to compare with each other, as they depend very much on the exact cell set-up, operating conditions and, in addition to the BPP used, also on the other cell components.

[1] More data on the conductivity and flexural strength of various metal and carbon materials can be found in Song et al. [33]

4 Summary

We present the characterization of a newly developed highly filled Ti composite material to be used as bipolar plates (BPP) in water electrolysis cells. Two- and three-dimensional microstructural analysis was performed to initially investigate the (surface) morphology, porosity and composition by SEM and X-ray micro-computed tomography of the different material compositions. The results explain well the qualitative trend of the surface roughness, the electrical conductivity and the flexural strength as a function of the metal to polymer ratio. Further correlations between the microstructure and macroscopic properties seem to exist and need to be analyzed in more detail.

The plates with an optimum Ti ratio of 80 wt.-% exhibit a remarkably high electrical conductivity for a composite of about 330 $(\Omega cm)^{-1}$. Even more, the mechanical and electrochemical characteristics also demonstrate their suitability as BPP with a flexural strength of about 30 MPa, a compressive strength of 100 MPa, and, with an additional titanium coating, a corrosion resistance comparable to that of pure titanium.

The water electrolysis test showed that the cell with the composite BPP achieved a cell voltage of about 2 V at a current density of 1 A at 80 °C, which is promising for this non-optimized material. The higher ohmic resistance on the anode side compared to the reference cell with the Ti BPP is due to insufficient corrosion protection and probably excessive surface roughness. These results give confidence that the performance of the cell can be further enhanced by improving the surface roughness and coating for better corrosion protection.

Our results show the possibility to produce alternative, not fully metallic BPP for water electrolysis. We were able to use less titanium and enable a faster and more effective fabrication of BPPs by hot pressing or injection molding.

Supplementary Information The online version contains supplementary material available at https://doi.org/10.1007/s00339-022-06304-3.

Acknowledgements The authors are thankful to Cristine Santos de Oliveira for preparation and 3D imaging of the samples by X-ray CT.

Funding Open Access funding enabled and organized by Projekt DEAL.

Declarations

Ethical statement This work was carried out within the "Bimeb" project which was founded by the program "Zentrale Innovationsprogramm Mittelstand (ZIM)" of the former German Federal Ministry of Economics under the identification code No. 16KN045250.

References

1. IEA, Global demand for pure hydrogen, 1975-2018. https://www.iea.org/data-and-statistics/charts/global-demand-for-pure-hydrogen-1975-2018
2. I.G.R. Outlook, *Energy transformation 2050* (Abu Dhabi, UAE, IRENA, 2020)
3. IEA, Global Hydrogen Review 2021. 2021; https://iea.blob.core.windows.net/assets/e57fd1ee-aac7-494d-a351-f2a4024909b4/GlobalHydrogenReview2021.pdf
4. E. Taibi, R. Miranda, W. Vanhoudt, T. Winkel, J.C. Lanoix, F. Barth. Hydrogen from renewable power: Technology outlook for the energy transition. **2018**,
5. IEA, The Future of Hydrogen. 2019; https://www.iea.org/reports/the-future-of-hydrogen
6. M. Crippa, G. Oreggioni, D. Guizzardi, M. Muntean, E. Schaaf, E. Lo Vullo, E. Solazzo, F. Monforti-Ferrario, J. Olivier, E. Vignati, Fossil CO2 and GHG emissions of all world countries: 2019 report; EUR; Publications Office of the European Union: Luxembourg, 2019; Vol. 29849
7. U. Babic, M. Suermann, F.N. Büchi, L. Gubler, T.J. Schmidt, Critical review-identifying critical gaps for polymer electrolyte water electrolysis development. J. Electrochem. Soc **164**, F387–F399 (2017)
8. P. Lettenmeier, A. S. Gago, K.A. Friedrich In New Technologies in Protective Coatings; Giudice, C., Canosa, G., Eds.; InTech: Rijeka, (2017)
9. M. Carmo, D.L. Fritz, J. Mergel, D. Stolten, A comprehensive review on PEM water electrolysis. Int. J. Hydrogen Energy **38**, 4901–4934 (2013)
10. L. Bertuccioli, A. Chan, D. Hart, F. Lehner, B. Madden, E. Standen,
11. M. Langemann, D.L. Fritz, M. Müller, D. Stolten, Validation and characterization of suitable materials for bipolar plates in PEM water electrolysis. Int. J. Hydrogen Energy **40**, 11385–11391 (2015)
12. M. Langemann, W. Lehnert, L. Singheiser, Bipolarplattenmaterialien für Polymer-Elektrolyt-Membran Elektrolyse. Ph.D. thesis, Universitätsbibliothek der RWTH Aachen, Aachen, (2016)
13. A.S. Gago, S.A. Ansar, B. Saruhan, U. Schulz, P. Lettenmeier, N.A. Cañas, P. Gazdzicki, T. Morawietz, R. Hiesgen, J. Arnold, K.A. Friedrich, Protective coatings on stainless steel bipolar plates for proton exchange membrane (PEM) electrolysers. J. Power Sourc. **307**, 815–825 (2016)
14. M.-T. Lin, C.-H. Wan, W. Wu, Characterization and corrosion resistance of TiZr coating on SS304 stainless steel using cathodic arc evaporation techniques. Surf. Coatings Technol. **320**, 217–225 (2017)
15. G. Chisholm, P.J. Kitson, N.D. Kirkaldy, L.G. Bloor, L. Cronin, 3D printed flow plates for the electrolysis of water:

An economic and adaptable approach to device manufacture. Energy Environ. Sci. **7**, 3026–3032 (2014)
16. G. Yang, J. Mo, Z. Kang, F.A. List, J.B. Green, S.S. Babu, F.-Y. Zhang, Additive manufactured bipolar plate for high-efficiency hydrogen production in proton exchange membrane electrolyzer cells. Int. J. Hydrogen Energy **42**, 14734–14740 (2017)
17. G. Yang, S. Yu, Z. Kang, Y. Dohrmann, G. Bender, B.S. Pivovar, J.B. Green, S.T. Retterer, D.A. Cullen, F.-Y. Zhang, A novel PEMEC with 3D printed non-conductive bipolar plate for low-cost hydrogen production from water electrolysis. Energy Convers. Manag. **182**, 108–116 (2019)
18. G. Wilhelm Sievers, K. Anklam, R. Henkel, T. Hickmann, V. Brüser, Corrosion-protection of moulded graphite conductive plastic bipolar plates in PEM electrolysis by plasma processing. Int. J. Hydrogen Energy **44**, 2435–2445 (2019)
19. F.G. Boyaci San, G. Tekin, A review of thermoplastic composites for bipolar plate applications. Int. J. Energy Res. **37**, 283–309 (2013)
20. R.A. Antunes, M.C.L. Oliveira, G. Ett, V. Ett, Corrosion of metal bipolar plates for PEM fuel cells: a review. Int. J. Hydrogen Energy **35**, 3632–3647 (2010)
21. A. Hermann, T. Chaudhuri, P. Spagnol, Bipolar plates for PEM fuel cells: a review. Int. J. Hydrogen Energy **30**, 1297–1302 (2005)
22. C. Minke, T. Hickmann, A.R. dos Santos, U. Kunz, T. Turek, Cost and performance prospects for composite bipolar plates in fuel cells and redox flow batteries. J. Power Sourc. **305**, 182–190 (2016)
23. M.G. Santarelli, M.F. Torchio, P. Cochis, Parameters estimation of a PEM fuel cell polarization curve and analysis of their behavior with temperature. J. Power Sourc. **159**, 824–835 (2006)
24. M. Newville, T. Stensitzki, D.B. Allen, A. Ingargiola, LMFIT: Non-Linear Least-Square Minimization and Curve-Fitting for Python. (2014)
25. B. Avasarala, P. Haldar, Effect of surface roughness of composite bipolar plates on the contact resistance of a proton exchange membrane fuel cell. J. Power Sourc. **188**, 225–229 (2009)
26. F.G. Boyacı San, O. Okur, The effect of compression molding parameters on the electrical and physical properties of polymer composite bipolar plates. Int. J. Hydrogen Energy **42**, 23054–23069 (2017)
27. D. Serban, C.G. Opran, Influence of the surface microstructure of conductive polymer composite bipolar plate on the fuel cell performance. Macromol. Symposia **396**, 2000324 (2021)
28. H.Y. Marghalani, Effect of filler particles on surface roughness of experimental composite series. J. Appl. Oral Sci. **18**, 59–67 (2010)
29. T.M. Besmann, J.J. Henry, E. Lara-Curzio, J.W. Klett, D. Haack, K. Butcher, Optimization of a Carbon Composite Bipolar Plate for PEM Fuel Cells. MRS Proceedings **2002**, 756
30. R.K. Upadhyay, A. Kumar, Effect of particle weight concentration on the lubrication properties of graphene based epoxy composites. Colloid Interface Sci. Commun. **33**, 100206 (2019)
31. N. Kim, S. Lienemann, I. Petsagkourakis, D. Alemu Mengistie, S. Kee, T. Ederth, V. Gueskine, P. Leclère, R. Lazzaroni, X. Crispin, K. Tybrandt, Elastic conducting polymer composites in thermoelectric modules. Nat. Commun. **11**, 1424 (2020)
32. U. S. Doe, The fuel cell technologies office multi-year research, development, and demonstration plan. US Department of Energy **2016**,
33. Y. Song, C. Zhang, C.-Y. Ling, M. Han, R.-Y. Yong, D. Sun, J. Chen, Review on current research of materials, fabrication and application for bipolar plate in proton exchange membrane fuel cell. Int. J. Hydrogen Energy **45**, 29832–29847 (2020)
34. W. Liao, F. Jiang, Y. Zhang, X. Zhou, Z. He, Highly-conductive composite bipolar plate based on ternary carbon materials and its performance in redox flow batteries. Renew. Energy **152**, 1310–1316 (2020)
35. H.-C. Kuan, C.-C.M. Ma, K.H. Chen, S.-M. Chen, Preparation, electrical, mechanical and thermal properties of composite bipolar plate for a fuel cell. J. Power Sourc. **134**, 7–17 (2004)
36. N.A. Mohd Radzuan, A.B. Sulong, J. Sahari, A review of electrical conductivity models for conductive polymer composite. Int. J. Hydrogen Energy **42**, 9262–9273 (2017)
37. Z. Bin, M. Bingchu, S. Chunhui, Y. Runzhang, Study on the electrical and mechanical properties of polyvinylidene fluroide/titanium silicon carbide composite bipolar plates. J. Power Sourc. **161**, 997–1001 (2006)
38. S. Chunhui, The effect of particle size gradation of conductive fillers on the conductivity and the flexural strength of composite bipolar plate. Int. J. Hydrogen Energy **33**, 1035–1039 (2008)
39. D. Prando, A. Brenna, M.V. Diamanti, S. Beretta, F. Bolzoni, M. Ormellese, M. Pedeferri, Corrosion of titanium: Part 1: aggressive environments and main forms of degradation. J. Appl. Biomater. Funct. Mater. **15**, e291–e302 (2017)
40. D.S. Falcão, A. Pinto, A review on PEM electrolyzer modelling: guidelines for beginners. J. Cleaner Prod. **261**, 121184 (2020)
41. T.A. Zawodzinski, T.E. Springer, F. Uribe, S. Gottesfeld, Characterization of polymer electrolytes for fuel cell applications. Solid State Ionics **60**, 199–211 (1993)
42. L. Liu, W. Chen, Y. Li, An overview of the proton conductivity of nafion membranes through a statistical analysis. J. Membr. Sci. **504**, 1–9 (2016)
43. H.-Y. Jung, S.-Y. Huang, B.N. Popov, High-durability titanium bipolar plate modified by electrochemical deposition of platinum for unitized regenerative fuel cell (URFC). J. Power Sourc. **195**, 1950–1956 (2010)